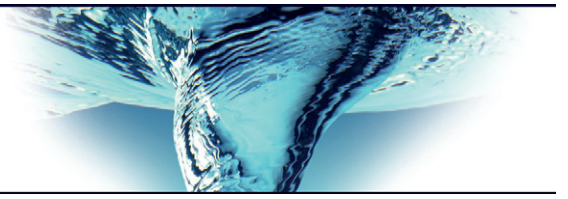
J. Fluid Mech. (2020), *vol.* 884, R3, doi:10.1017/jfm.2019.990



JFM RAPIDS
journals.cambridge.org/rapids

Streaky dynamo equilibria persisting at infinite Reynolds numbers

Kengo Deguchi†

School of Mathematics, Monash University, VIC 3800, Australia

(Received 22 September 2019; revised 7 November 2019; accepted 8 November 2019)

Nonlinear three-dimensional dynamo equilibrium solutions of viscous-resistive magneto-hydrodynamic equations are continued to formally infinite magnetic and hydrodynamic Reynolds numbers. The external driving mechanism of the dynamo is a uniform shear, which constitutes the base laminar flow and cannot support any kinematic dynamo. Nevertheless, an efficient subcritical nonlinear instability mechanism is found to be able to generate large-scale coherent structures known as streaks, for both velocity and magnetic fields. A finite amount of magnetic field generation is identified at the self-consistent asymptotic limit of the nonlinear solutions, thereby confirming the existence of an effective nonlinear dynamo action at astronomically large Reynolds numbers.

Key words: high-speed flow, dynamo theory, bifurcation

1. Introduction

Almost exactly one century ago, Larmor envisioned that the magnetic field observed in the Universe is self-excited through a motion of electrically conducting fluids (Larmor 1919). Generating a magnetic field via the kinematic–magnetic energy conversion like a mechanical dynamo looked like a simple task at first glance given the coupling of the velocity and magnetic fields in the magneto-hydrodynamic (MHD) equations. However, despite the intensive theoretical, numerical and experimental studies over a hundred years, many problems remain open in this area of research.

One of the biggest concerns in dynamo studies is whether the energy conversion remains effective at extremely large magnetic Reynolds number R_m of astrophysical interest. Finding kinematic dynamos with finite positive growth rate (so-called fast dynamos) was a major goal in the early years of highly idealised model flow studies (Childress & Gilbert 1995), while the recent state-of-the-art simulations by Yousef *et al.* (2008*a*) found that kinematic dynamos can be supported by a simple shear, which naturally presents in various physical situations (for example, stellar interiors,

† Email address for correspondence: kengo.deguchi@monash.edu

© Cambridge University Press 2019

https://doi.org/10.1017/jfm.2019.990 Published online by Cambridge University Press

laboratory dynamos and solar atmospheres, see Ossendrijver (2003), Monchaux *et al.* (2007), Charbonneau (2014) also). The R_m used in Yousef *et al.* (2008*a*) was very small. The subsequent kinematic and nonlinear shear dynamo simulations by Tobias & Cattaneo (2013) and Teed & Proctor (2017) then uncovered that the large-scale coherent structures within turbulent flows are ultimately responsible for magnetic field generation even at moderately high R_m. However, the advances in computing technology have not yet allowed us to reach the R_m of typical solar/stellar dynamos.

The computational difficulty in particular at the nonlinear stage essentially comes from the multi-scale and chaotic nature of turbulence. Turbulent flow simulations of real-world problems must rely greatly on phenomenological turbulent models, while researchers who seek to make a reduced model with a mean–fluctuation decomposition always encounter the closure problem, where no mathematically justified procedure is available. In general, whether effective nonlinear dynamo coherent structures exist at astronomically large R_m remains a fundamental question in the dynamo study; see the latest excellent review paper by Rincon (2019), for example.

Towards the end of the 20th century, the dynamical systems theory approach spread among hydrodynamicists who hoped to analyse coherent structures in turbulence without using any *ad hoc* assumption. In this approach, turbulence is understood as a chaotic trajectory wandering around a complicated network formed by unstable solutions whose properties are invariant in time (for example, steady equilibrium solutions, travelling wave solutions, periodic orbits); see Waleffe (1997), Gibson, Halcrow & Cvitanovic (2008), Kawahara, Uhlmann & van Veen (2012) and Willis, Cvitanovic & Avila (2013). Even shear flows with a simple configuration could support three-dimensional equilibrium solutions, as first found in plane Couette flow by Nagata (1990) and Clever & Busse (1992). It has been repeatedly shown that the flow fields of the invariant solutions are remarkably reminiscent of large-scale coherent structures observed in turbulent simulations and experiments (Hamilton, Kim & Waleffe 1995; Hof *et al.* 2004). More recently, there has also been a great deal of dynamical-systems-theory-based research on nonlinear shear-driven MHD dynamos under Kepler rotation, although the studies are limited to relatively small R_m (Rincon, Ogilvie & Proctor 2007; Herault *et al.* 2011; Riols *et al.* 2013). Deguchi (2019*a*,*b*) theoretically and numerically showed that, at least for the non-rotating case, the large-R_m dynamo solution branch obeys a clean asymptotic law. However, the generated magnetic field is unfortunately found to become asymptotically small at the large-R_m limit.

Our goal in this paper is twofold. One, compute a new equilibrium dynamo solution in the infinite-R_m limit for a simple shear flow. Two, use that limiting equilibrium solution to confirm the generation of a finite magnetic field amplitude at asymptotically large R_m. In the next section, we begin by presenting the mathematical formulation of the problem. In § 3 we shall first generate a nonlinear dynamo solution branch by a bifurcation from the subcritical three-dimensional hydrodynamic plane Couette flow solution mentioned above, and then theoretically and numerically analyse their large-Reynolds-number fate. The results are summarised in § 4 with a brief discussion.

2. Formulation of the problem

It will become clear that the theoretical framework to be developed in this study can be applicable for a quite wide range of MHD flows. However, it is advantageous to choose the flow configuration as simple as possible in order to concisely describe the

https://doi.org/10.1017/jfm.2019.990 Published online by Cambridge University Press

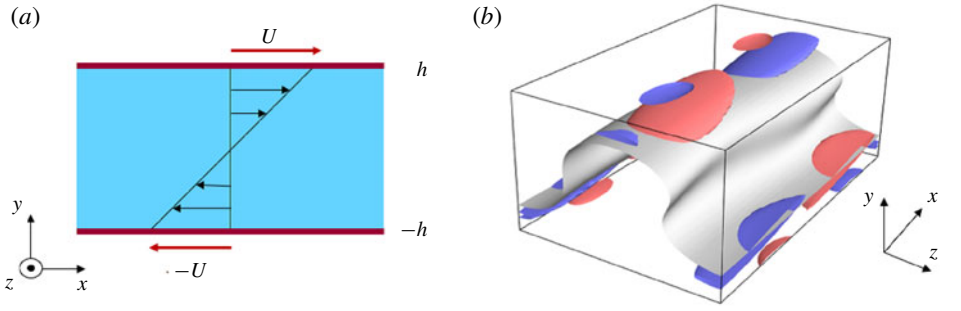


FIGURE 1. (*a*) Configuration of dimensional plane Couette flow and its laminar solution. (*b*) The nonlinear steady plane Couette flow solution due to Nagata (1990), Clever & Busse (1992). $R = 236.4$. The box size is $[0, 2\pi/\alpha] \times [-1, 1] \times [0, \pi]$, where $\alpha = 300/R \approx 1.27$. The solution is purely hydrodynamic, and corresponds to the green dot at $\epsilon = 1.79 \times 10^{-5}$ in figure 2. The streak structure is shown by the grey isosurface of zero streamwise velocity. The red and blue isosurfaces illustrate the streamwise vorticity by showing 70 % of the maximum and minimum values, respectively.

main point of the theory and the computational methodology. The flow configuration we select for this purpose is plane Couette flow, a flow between two mutually moving parallel walls; see figure 1(*a*). Choosing the wall speed U and the half-gap h as the velocity and the length scales, respectively, the non-dimensional MHD equations can be written as

$$\frac{\mathrm{D}\boldsymbol{u}}{\mathrm{D}t} - (\boldsymbol{b}\cdot\boldsymbol{\nabla})\boldsymbol{b} = -\boldsymbol{\nabla}p + \frac{1}{R}\nabla^2\boldsymbol{u}, \quad \boldsymbol{\nabla}\cdot\boldsymbol{u} = 0, \tag{2.1}$$

$$\frac{\mathrm{D}\boldsymbol{b}}{\mathrm{D}t} - (\boldsymbol{b}\cdot\boldsymbol{\nabla})\boldsymbol{u} = \frac{1}{R_m}\nabla^2\boldsymbol{b}, \quad \boldsymbol{\nabla}\cdot\boldsymbol{b} = 0. \tag{2.2}$$

Here $\boldsymbol{\nabla} = (\partial_x, \partial_y, \partial_z)$ is the gradient in the Cartesian coordinates and $\mathrm{D}/\mathrm{D}t = \partial_t + (\boldsymbol{u}\cdot\boldsymbol{\nabla})$ is the material derivative. Note that for the magnetic field, the corresponding Alfvén wave speed is non-dimensionalised by the velocity scale. The first set of equations are the Navier–Stokes equations, which represent the conservation of momentum and mass, while the second set of equations are found from the Maxwell equations and Ohm's law. Kinematic dynamo studies assume the smallness of the magnetic field $\boldsymbol{b} = (b_x, b_y, b_z)$ so that the Lorentz force term $(\boldsymbol{b}\cdot\boldsymbol{\nabla})\boldsymbol{b}$ is negligible in (2.1). In that case, the magnetic field is found from a linear analysis of (2.2), because the velocity $\boldsymbol{u} = (u_x, u_y, u_z)$ and the pressure p are determined from (2.1). As our interest here is the amplitude of the magnetic field, fully nonlinear analysis is necessary.

The magnetic and hydrodynamic Reynolds numbers are defined as $R_m = Uh/\eta$ and $R = Uh/\nu$, respectively, using the kinematic viscosity ν and Ohmic diffusivity η of the fluid. The flow is assumed to be periodic in both $x \in [0, 2\pi/\alpha]$ and $z \in [0, \pi]$, with the streamwise wavenumber α. The box dimensions seen in figure 1(*b*) are close to those used in Hamilton *et al.* (1995), and as seen in that paper, typically only one streak is generated in the flow. The walls at $y = \pm 1$ are no-slip, and either perfectly conducting or insulating (Roberts 1964). Dynamos are self-excited MHD solutions, so any external magnetic effects must be switched off. We do not use the small-scale isotropic, non-helical external forcing term used in the majority of shear-driven

https://doi.org/10.1017/jfm.2019.990 Published online by Cambridge University Press

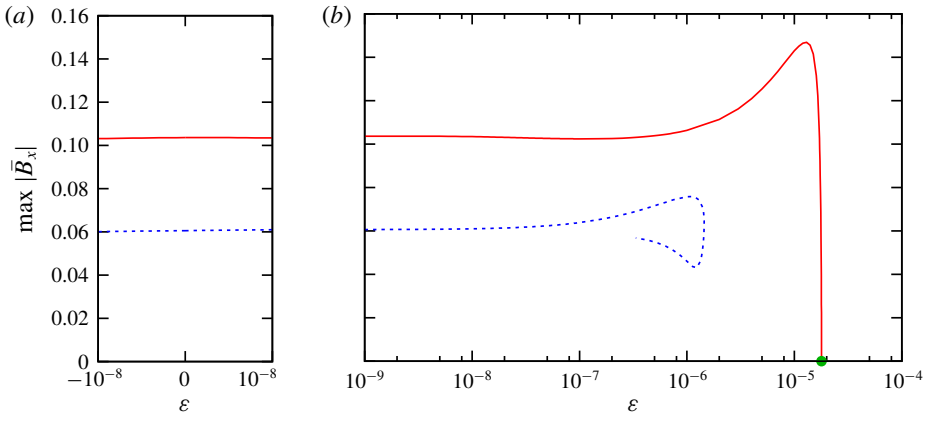


FIGURE 2. Bifurcation diagram of the dynamo solution branches. Here $\alpha_0 \equiv \alpha R_m = 300$ and $P_m = 1$. Red solid curve: perfectly conducting walls. Blue dashed curve: perfectly insulating walls. The green dot corresponds to the pitchfork bifurcation point where the red branch emanates from the kinematic dynamo action on top of the streaky field shown in figure 1(*b*). Panel (*a*) shows that both branches can be continued towards the infinite-Reynolds-number limit ($\epsilon = 0$). The solutions for $\epsilon < 0$ do not have any physical meaning; see (3.1).

dynamo studies (Yousef *et al.* 2008*a*,*b*; Tobias & Cattaneo 2013; Teed & Proctor 2017). Therefore, the only mechanism of energy input to the system is the shear due to the movement of the walls.

The system has the laminar Couette flow solution $\boldsymbol{u} = (y, 0, 0), \boldsymbol{b} = (0, 0, 0)$. There is no linear instability at all in this flow, unlike cylindrical (Willis & Barenghi 2002) or spherical (Guervilly & Cardin 2010) Couette dynamo problems. The proof is simple. First, we note that Squire's theorem is applicable even when magnetic effects are present, and thus it is sufficient to look for z-independent two-dimensional perturbation (Squire 1933; Drazin & Reid 1981). Then from the Zel'dovich theorem (Zel'dovich 1957), there is no exponentially growing magnetic perturbations. Finally, as shown by Romanov (1973), there is no linear instability for purely hydrodynamic plane Couette flow.

Transition to turbulence nonetheless occurs by finite-amplitude perturbations (Nauman & Blackman 2017). For the purely hydrodynamic case $\boldsymbol{b} \equiv \boldsymbol{0}$, the non-trivial steady solution found in Nagata (1990) and Clever & Busse (1992) is responsible for this subcritical transition; here we reproduce the same solution in figure 1(*b*). The flow field of the solution is characterised by streaks – namely, inhomogeneity of the streamwise velocity swept by the streamwise vortices. A detailed description of the numerical code used can be found in Deguchi, Hall & Walton (2013) and Deguchi (2019*b*). The scheme first discretises (2.1) and (2.2) by means of the spectral method, and then Newton's method is applied to find steady unstable solutions. To produce a reliable numerical result, up to 12 and 30 Fourier harmonics are taken in x and z, respectively, while 70 Chebyshev modes are used in y.

3. Theoretical and numerical analyses

The streak field for example seen in figure 1(*b*) is three-dimensional and hence can support a kinematic dynamo action, whose onset provides the bifurcation

https://doi.org/10.1017/jfm.2019.990 Published online by Cambridge University Press

point of nonlinear dynamo solution branches. Throughout our computations the magnetic Prandtl number $P_m = R_m/R = \nu/\eta$ is fixed to be unity. Also the streamwise wavenumber is set to be $\alpha = 300/R$ for later convenience, unless otherwise specified. The bifurcation diagram shown in figure 2 can best illustrate the emergence of the dynamo solution branches. Here we measure the magnetic field amplitude by the maximum of $|\overline{B}_x|$, where $\overline{B}_x(y)$ is the streamwise magnetic field averaged in x and z. The horizontal axis is

$$\epsilon = R_m^{-2}. \tag{3.1}$$

We shall shortly see that the introduction of this small parameter is the key to reaching our goals.

When the walls are perfectly conducting, the kinematic dynamo problem (2.2) possesses a real eigenvalue, which passes thorough zero at $R = 236.4$; that is, the parameter used in figure 1(*b*). This solution corresponds to the green point at $\epsilon = 1.79 \times 10^{-5}$ in figure 2. The red curve is one of the dynamo solution branches produced by the pitchfork bifurcation at this point. The other dynamo solution branch exactly overlaps this curve because of the transformation $\boldsymbol{b} \to -\boldsymbol{b}$ mapping one solution to the other; equations (2.1) and (2.2) are invariant under this transformation because the magnetic field is a pseudo-vector in the MHD framework.

An alternative way to obtain a dynamo solution is by seeking nonlinear solutions to an externally magnetised system and then examining the limit of vanishing external magnetic field. This approach resulted in a successful strategy for perfectly insulating walls in the previous study (Deguchi 2019*a*,*b*); the corresponding dynamo solution branch is shown by the blue dashed curve in figure 2.

Having determined nonlinear dynamo solution branches, we will now continue them to the large-R_m limit. Because of the choice $P_m = 1$, this limit corresponds also to the large-R limit. We begin the analysis by applying the long-wavelength rescaling

$$x = R_m X \tag{3.2}$$

with

$$(u_x, u_y, u_z, p) = (U_x, R_m^{-1}U_y, R_m^{-1}U_z, R_m^{-2}P), \tag{3.3}$$

$$(b_x, b_y, b_z) = (B_x, R_m^{-1}B_y, R_m^{-1}B_z), \tag{3.4}$$

which makes the steady version of (2.1) and (2.2) take the form

$$(\boldsymbol{U}\cdot\nabla)\boldsymbol{U} - (\boldsymbol{B}\cdot\nabla)\boldsymbol{B} = -\nabla_\epsilon P + P_m\triangle_\epsilon \boldsymbol{U}, \quad \nabla\cdot\boldsymbol{U} = 0, \tag{3.5}$$

$$(\boldsymbol{U}\cdot\nabla)\boldsymbol{B} - (\boldsymbol{B}\cdot\nabla)\boldsymbol{U} = \triangle_\epsilon \boldsymbol{B}, \quad \nabla\cdot\boldsymbol{B} = 0. \tag{3.6}$$

Here ∇ is redefined as $(\partial_X, \partial_y, \partial_z)$, and

$$\nabla_\epsilon = (\epsilon\partial_X, \partial_y, \partial_z), \quad \triangle_\epsilon = \epsilon\partial_X^2 + \partial_y^2 + \partial_z^2. \tag{3.7a,b}$$

Note that no approximation has been made at this stage. In the rescaled coordinate, the flow is periodic in $[0, 2\pi/\alpha R_m]$, so we define the rescaled wavenumber $\alpha_0 = \alpha R_m$, where $\alpha_0 = 300$.

The underlying motivation behind the scaling is somewhat similar to Prandtl's boundary layer theory; more precisely, equations (3.5) and (3.6) at the limit $\epsilon \to 0$ are similar to the so-called 'boundary region equations', used in the boundary layer

https://doi.org/10.1017/jfm.2019.990 Published online by Cambridge University Press

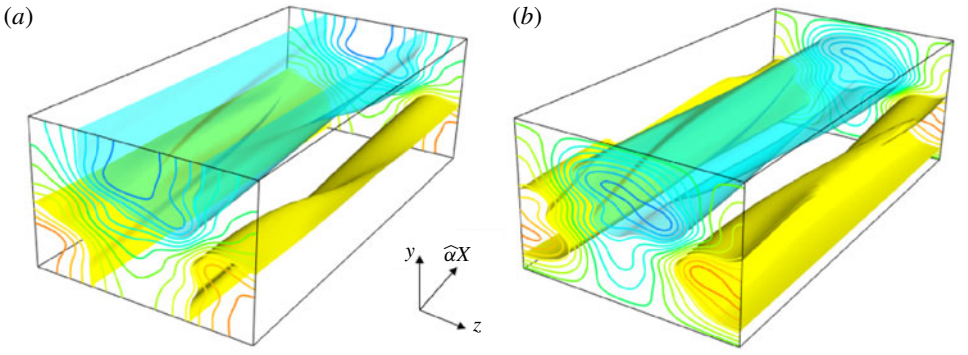


FIGURE 3. The streamwise magnetic field generated at infinite Reynolds number ($\epsilon = 0$ in figure 2). $\alpha_0 \equiv \alpha R_m = 300$ and $P_m = 1$. The box size is $[0, 2\pi] \times [-1, 1] \times [0, \pi]$. The yellow/blue surfaces are the isosurface of 50 % of the maximum/minimum, respectively. (*a*) Perfectly conducting walls. (*b*) Perfectly insulating walls.

and microchannel flow studies (Kemp 1951; Fletcher 1988; Hall 1988; Rubin & Tannehill 1992; Deguchi *et al.* 2013). With this scaling, some diffusive terms are still retained even at the large-Reynolds-number limit. This is because the driving mechanisms brought about by the shear are multiplied by the x derivative, which is small from (3.2); hence the viscous–convective balance is always achieved. This diffusivity allows us to continue the solution branch across $\epsilon = 0$, as shown in figure 2. In fact, the streamwise magnetic field shown in figure 3 suggests that the limiting flow field remains nicely smooth.

There is one minor technical remark that should be made here. If one uses the toroidal–poloidal potential decomposition for the flow field, some special care must be taken in the scaling of the potentials to avoid the singularity of the Jacobian matrix at $\epsilon = 0$; see Deguchi *et al.* (2013). Alternatively, one can confirm that the initial guess created by a linear interpolation of nearby two solutions (at $\epsilon = 10^{-12}$ and -10^{-12}, say) gives a very small residue with which the input data can be accepted as an accurate solution.

The streaky hydrodynamic flow structure is qualitatively unchanged from that shown in figure 1(*b*), while the examination of figure 3 indicates that the generated magnetic field also forms a streaklike structure. The dynamo solution inherits the two symmetries seen in the hydrodynamic plane Couette solution (Nagata 1990; Clever & Busse 1992)

$$\begin{aligned}[u_x, u_y, u_z](x, y, z) &= [-u_x, -u_y, u_z](-x, -y, z + \pi/2) \\ &= [u_x, u_y, -u_z](x + \pi/\alpha, y, -z),\end{aligned} \tag{3.8}$$

with the same symmetries satisfied for the magnetic field. It is widely acknowledged in hydrodynamic studies that the latter shift–reflection symmetry is responsible for the sinusoidal meandering of the streak. The transformation (3.2) implies that, for large enough R_m, streamwise development of the flow is so slow that it may locally look almost two-dimensional. However, that streamwise modulation is nevertheless crucial in sustaining the dynamo mechanism because if it is absent there should be no dynamo solution from the parallel flow manifestation of Cowling's antidynamo theorem (Cowling 1934).

https://doi.org/10.1017/jfm.2019.990 Published online by Cambridge University Press

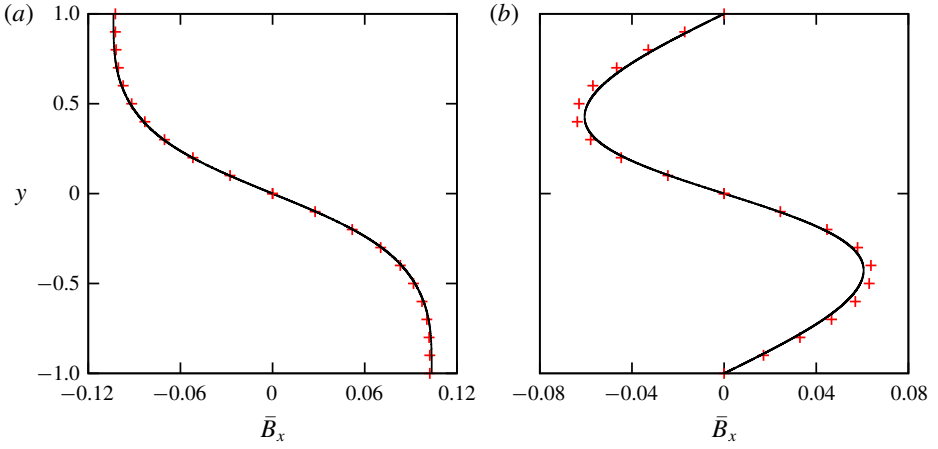


FIGURE 4. The generated mean magnetic field for $\alpha_0 = 300$. The solid curve is the limiting result (the same solutions as figure 3). The red points are the finite-Reynolds-number result at $R_m = R = 3000$. (*a*) Perfectly conducting walls. (*b*) Perfectly insulating walls.

The flow field quickly converges to the limiting result with increasing R_m. Figure 4 compares the mean magnetic field $\bar{B}_x$ of the limiting and finite-Reynolds-number solutions. Even at R_m as low as order 10^3, the two results are very close to each other. At higher R_m, of order 10^4, the finite-Reynolds-number result is graphically indistinguishable from the limiting result.

The reason for the rapid convergence can be explained by the formal asymptotic analysis. We first remark here that the large-Reynolds-number limit is a singular perturbation problem, where the ideal (diffusionless) problem may not produce the same result as the $R_m^{-1} \to 0$ limit of the diffusive problem. The diffusion effect is in fact not negligible when the flow develops a small-scale structure. This is the reason why the formal asymptotic analysis of high-Reynolds-number flows usually involves complicated matched asymptotic expansions.

Having said that, the rescaled system of (3.5)–(3.6) admits the regular asymptotic expansions

$$\boldsymbol{U} = \boldsymbol{U}_0(X, y, z) + \epsilon \boldsymbol{U}_1(X, y, z) + O(\epsilon^2), \tag{3.9}$$

$$\boldsymbol{B} = \boldsymbol{B}_0(X, y, z) + \epsilon \boldsymbol{B}_1(X, y, z) + O(\epsilon^2), \tag{3.10}$$

$$P = P_0(X, y, z) + \epsilon P_1(X, y, z) + O(\epsilon^2), \tag{3.11}$$

for small ϵ. The crux of the argument is that, in our particular equilibrium invariant solutions, all the small-scale structures are screened out. As was mentioned in § 1, the solutions satisfy the MHD equations exactly within numerical accuracy, and hence, in this sense, there is no model reduction necessary to isolate large-scale coherent structures.

The leading-order solution $(\boldsymbol{U}_0, \boldsymbol{B}_0, P_0)$ is what we found by letting $\epsilon \to 0$ in the rescaled system of (3.5)–(3.6). The correction to the leading-order part is of $O(\epsilon)$, which is numerically very small even at moderately high R_m. Clearly, the scaling (3.4) and the asymptotic expansions (3.10) indicate that the streamwise magnetic field eventually becomes independent of R_m. Therefore, the generated magnetic field is, indeed, finite at the asymptotic limit.

https://doi.org/10.1017/jfm.2019.990 Published online by Cambridge University Press

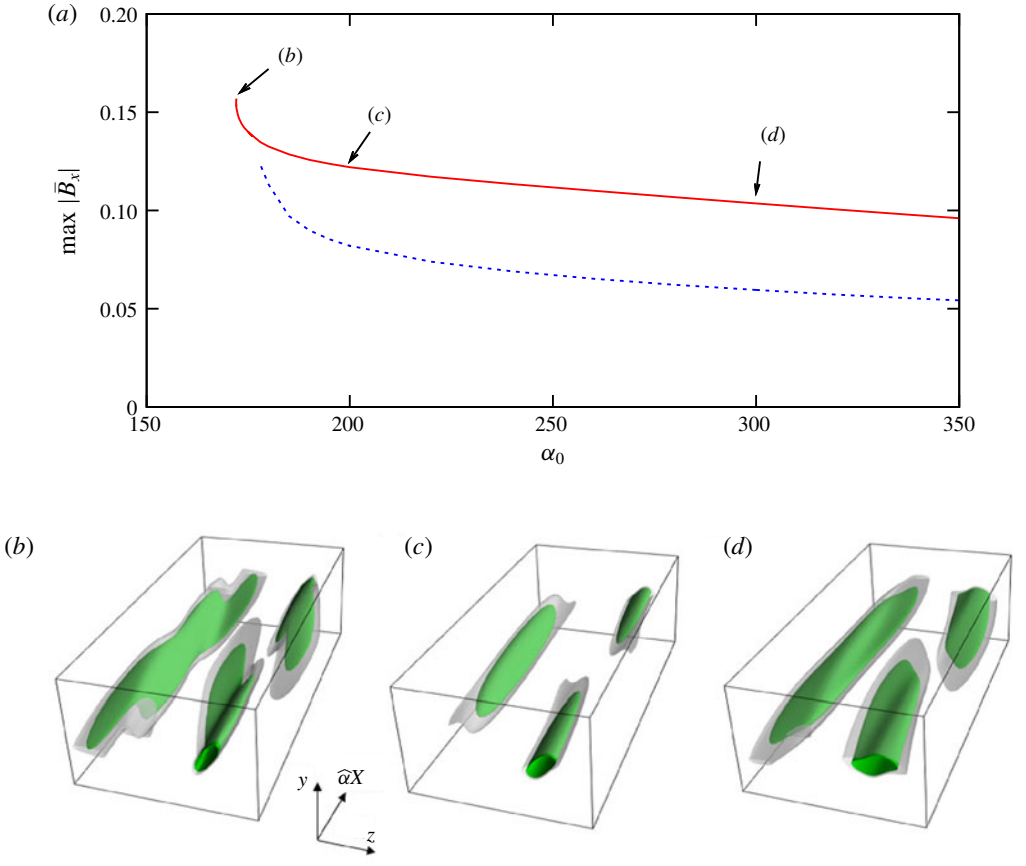


FIGURE 5. (*a*) The α_0 dependence of the limiting dynamo solutions ($\epsilon = 0$, $P_m = 1$). Red solid curve: perfectly conducting walls. Blue dashed curve: perfectly insulating walls. (*b–d*) Visualisation of the electric current strength $|\boldsymbol{j}|$ generated by the corresponding dynamo solutions indicated in (*a*). Grey transparent/green surface represents 50 %/60 % maximum value.

The strength of the dynamo action gets stronger with decreasing α_0, as shown in figure 5(*a*). For large α_0, on the other hand, the dynamo becomes less effective; this observation is certainly consistent with Deguchi (2019*a*,*b*), where theoretical and numerical evidence was given for the $O(\epsilon^{1/6})$ magnetic field generation at the shorter wavelength $\alpha = O(1)$. Note also that in Deguchi (2019*b*) the asymptotic problem is solved with a regularisation effect whose strength is controlled by a parameter. On the other hand, the asymptotic problem obtained in this paper does not require such regularisation.

The electric current $\boldsymbol{j} = \nabla \times \boldsymbol{b}$ produced by the dynamo mechanism is also $O(\epsilon^0)$. In figure 5(*b–d*) we use the magnitude of it to see the α_0 dependence of the field structure of the dynamos. The green blobs enclosing the region where the strong current is generated are shortened in the streamwise direction for smaller α_0; compare figure 5(*d*) for $\alpha_0 = 300$ and figure 5(*c*) for $\alpha_0 = 200$. That streamwise concentration of the structure affects the decay of the streamwise Fourier coefficients, and hence the computation was double-checked using 18 streamwise Fourier modes.

https://doi.org/10.1017/jfm.2019.990 Published online by Cambridge University Press

The convergence problem becomes even more serious on approaching the saddle-node point (b), because of the complicated field structure developed in all three directions. We are unable to determine if it is possible to round the saddle-node point. Note that, unlike finite-Reynolds-number computations, the solution branch of an asymptotically reduced problem may be terminated due to a mathematical singularity; see Dempsey *et al.* (2016) for example.

4. Summary and discussion

We have demonstrated that there are self-consistent, subcritical, nonlinear and three-dimensional dynamo solutions that persist at infinite hydrodynamic and magnetic Reynolds numbers. The homogeneous shear, which is used as an external base driving mechanism of the dynamos, presents as a large-scale background structure in many real-world problems (Ossendrijver 2003; Monchaux *et al.* 2007; Charbonneau 2014; Rincon 2019). Although such base flows may be stable with respect to small perturbations, finite-amplitude dynamos can be driven indirectly via the three-dimensional nonlinear mechanism. The key to the successful computation of the dynamos at the large-Reynolds-number limit is the method of invariant solutions, which allows us to isolate the large-scale structure without any *ad hoc* assumptions. The nonlinear dynamo solutions found are almost always unstable. As established in many previous purely hydrodynamic and magneto-hydrodynamic studies, at least for the transitional regime, such unstable solutions typically constitute a mathematically rational 'backbone' on which large-scale coherent structures in turbulence hang (Hamilton *et al.* 1995; Waleffe 1997; Hof *et al.* 2004; Rincon *et al.* 2007; Gibson *et al.* 2008; Herault *et al.* 2011; Kawahara *et al.* 2012; Riols *et al.* 2013; Willis *et al.* 2013).

The finite-amplitude dynamo magnetic field generation at the large-R_m limit has been conclusively determined for the first time, within a framework that is fully consistent to the asymptotic behaviour of the finite-R_m results. The rapid convergence of the finite-Reynolds-number results towards the limiting result is justified by the asymptotic analysis. The numerical limiting process has been proved successful for the two popularly used magnetic boundary conditions on the walls. Thus we expect that the effective streaky magnetic field generation mechanism is robust against the flow configuration, so that a similar structure may also appear in various MHD flows.

There are some astrophysical flows where the present method could be applicable, but with some extensions. Threadlike structures reminiscent of the streak can for example be found in the observation of the Sun's atmosphere (Okamoto *et al.* 2015). For such atmospheric flows the effects of compressibility and stratification must be included to find quantitative features of the dynamos. Streaklike subcritical dynamos have also been observed in shear flows under Kepler rotation, and believed to play an important role in angular momentum transport of accretion disks (Rincon *et al.* 2007; Herault *et al.* 2011; Riols *et al.* 2013). At least it was numerically confirmed for moderate R_m that the shear-driven dynamo obtained in Yousef *et al.* (2008*a*) works even for the rotating case (Yousef *et al.* 2008*b*). More recently, the existence of similar subcritical dynamos in global cylindrical coordinate simulations has been reported by Guseva *et al.* (2017). In cylindrical geometry, there is a maximal length scale in the streamwise (azimuthal) direction. This means that the cross-streamwise scale of the coherent structures must be small in order to apply the scaling of the dynamos discussed in this paper.

The present study focused only on $P_m = 1$. The question therefore naturally arises as to how the magnetic field generation changes as that parameter varies. Within the

https://doi.org/10.1017/jfm.2019.990 Published online by Cambridge University Press

asymptotic framework, P_m is formally an $O(\epsilon^0)$ quantity. Thus the range of P_m within which the large-R_m dynamos exist must be studied numerically in the future. The value of P_m in plasma flows changes depending on the temperature and density; for example, the recent plasma experiment used noble gases to control P_m within the range 0.2–12 (Collins *et al.* 2014). The tentative calculations suggest that certainly our limiting dynamo solutions exist for the relevant range of P_m. This result may motivate experimentalists to use a plasma flow as simple as that through a long straight pipe to generate a strong streaky magnetic field. Such experiments may help answering the question whether the invariant solutions remain relevant to turbulent dynamics at large R_m and R, beyond the transitional regime.

Acknowledgements

This work was supported by Australian Research Council Discovery Early Career Researcher Award DE170100171.

Declaration of interests

The authors report no conflict of interest.

References

CHARBONNEAU, P. 2014 Solar dynamo theory. *Annu. Rev. Astron. Astrophys.* **94**, 39–48.

CHILDRESS, S. & GILBERT, A. D. 1995 *Stretch, Twist, Fold: The Fast Dynamo*. Springer.

CLEVER, R. M. & BUSSE, F. H. 1992 Three-dimensional convection in a horizontal fluid layer subjected to a constant shear. *J. Fluid Mech.* **234**, 511–527.

COLLINS, C., CLARK, M., COOPER, C. M., FLANAGAN, K., KHALZOV, I. V., NORNBERG, M. D., SEIDLITZ, B., WALLACE, J. & FOREST, C. B. 2014 Taylor–Couette flow of unmagnetized plasma. *Phys. Plasmas* **21**, 42–117.

COWLING, T. G. 1934 The magnetic fields of sunspots. *Mon. Not. R. Astron. Soc.* **94**, 39–48.

DEGUCHI, K. 2019*a* High-speed shear-driven dynamos. Part 1. Asymptotic analysis. *J. Fluid Mech.* **868**, 176–211.

DEGUCHI, K. 2019*b* High-speed shear-driven dynamos. Part 2. Numerical analysis. *J. Fluid Mech.* **876**, 830–858.

DEGUCHI, K., HALL, P. & WALTON, A. G. 2013 The emergence of localized vortex–wave interaction states in plane Couette flow. *J. Fluid Mech.* **721**, 58–85.

DEMPSEY, L. J., DEGUCHI, K., HALL, P. & WALTON, A. G. 2016 Localized vortex/Tollmien–Schlichting wave interaction states in plane Poiseuille flow. *J. Fluid Mech.* **791**, 97–121.

DRAZIN, P. G. & REID, W. H. 1981 *Hydrodynamic Stability*. Cambridge University Press.

FLETCHER, C. A. J. 1988 *Computational Techniques for Fluid Dynamics*. Springer.

GIBSON, J. F., HALCROW, J. & CVITANOVIC, P. 2008 Visualizing the geometry of state space in plane Couette flow. *J. Fluid Mech.* **611**, 107–130.

GUERVILLY, C. & CARDIN, P. 2010 Numerical simulations of dynamos generated in spherical Couette flows. *Geophys. Astrophys. Fluid Dyn.* **104**, 221–248.

GUSEVA, A., HOLLERBACH, R., WILLIS, A. P. & AVILA, M. 2017 Dynamo action in a quasi-Keplerian Taylor–Couette flow. *Phys. Rev. Lett.* **119**, 164501.

HALL, P. 1988 The nonlinear development of Görtler vortices in growing boundary layers. *J. Fluid Mech.* **193**, 243–266.

HAMILTON, J. M., KIM, J. & WALEFFE, F. 1995 Regeneration mechanisms of near-wall turbulence structures. *J. Fluid Mech.* **287**, 317–348.

HERAULT, J., RINCON, F., COSSU, C., LESUR, G., OGILVIE, G. I. & LONGARETTI, P.-Y. 2011 Periodic magneto rotational dynamo action as a prototype of nonlinear magnetic field generation in shear flows. *Phys. Rev.* E **84**, 036321.

https://doi.org/10.1017/jfm.2019.990 Published online by Cambridge University Press

HOF, B., VAN DOORNE, C. W., WESTERWEEL, J., NIEUWSTADT, F. T., FAISST, H., ECKHARDT, B., WEDIN, H., KERSWELL, R. R. & WALEFFE, F. 2004 Experimental observation of nonlinear traveling waves in turbulent pipe flow. *Science* **305** (5690), 1594–1598.

KAWAHARA, G., UHLMANN, M. & VAN VEEN, L. 2012 The significance of simple invariant solutions in turbulent flows. *Annu. Rev. Fluid Mech.* **44**, 203–225.

KEMP, N. 1951 The laminar three-dimensional boundary layer and a study of the flow past a side edge. M.Ac.S Thesis, Cornell University, Ithaca, NY.

LARMOR, J. 1919 How could a rotating body such as the sun become a magnet. *Rep. Brit. Assoc. Adv. Sci.* **87**, 159–160.

MONCHAUX, R., BERHANU, M., BOURGOIN, M., MOULIN, M., ODIER, PH., PINTON, J.-F., VOLK, R., FAUVE, S., MORDANT, N., PÉTRÉLIS, F. *et al.* 2007 Generation of a magnetic field by dynamo action in a turbulent flow of liquid sodium. *Phys. Rev. Lett.* **98**, 044502.

NAGATA, M. 1990 Three-dimensional finite-amplitude solutions in plane Couette flow: bifurcation from infinity. *J. Fluid Mech.* **217**, 519–527.

NAUMAN, F. & BLACKMAN, E. G. 2017 Sustained turbulence and magnetic energy in nonrotating shear flows. *Phys. Rev.* E **95**, 033202.

OKAMOTO, T. J., ANTOLIN, P., DE PONTIEU, B., UITENBROEK, H., VAN DOORSSELAERE, T. & YOKOYAMA, T. 2015 Resonant absorption of transverse oscillations and associated heating in a solar prominence. Part I. Observational aspects. *Astrophys. J.* **809** (71), 1–12.

OSSENDRIJVER, M. 2003 The solar dynamo. *Astron. Astrophys. Rev.* **11**, 287–367.

RINCON, F. 2019 Dynamo theories. *J. Plasma Phys.* **85**, 205850401.

RINCON, F., OGILVIE, G. I. & PROCTOR, M. R. E. 2007 Self-sustaining nonlinear dynamo process in Keplerian shear flows. *Phys. Rev. Lett.* **98**, 254502.

RIOLS, A., RINCON, F., COSSU, C., LESUR, G., LONGARETTI, P.-Y., OGILVIE, G. I. & HERAULT, J. 2013 Global bifurcations to subcritical magnetorotational dynamo action in Keplerian shear flow. *J. Fluid Mech.* **731**, 1–45.

ROBERTS, P. H. 1964 The stability of hydromagnetic Couette flow. *Proc. Camb. Phil. Soc.* **60**, 635–651.

ROMANOV, V. A. 1973 Stability of plane-parallel Couette flow. *Funct. Anal. Applics* **7**, 137–146.

RUBIN, S. G. & TANNEHILL, J. C. 1992 Parabolized/reduced Navier–Stokes computational techniques. *Annu. Rev. Fluid Mech.* **24**, 117–144.

SQUIRE, H. B. 1933 On the stability for three-dimensional disturbances of viscous fluid flow between parallel walls. *Proc. R. Soc. Lond.* A **142** (847), 621–628.

TOBIAS, S. M. & CATTANEO, F. 2013 Shear-driven dynamo waves at high magnetic Reynolds number. *Nature* **497**, 463–465.

TEED, R. J. & PROCTOR, M. R. E. 2017 Quasi-cyclic behaviour in non-linear simulations of the shear dynamo. *Mon. Not. R. Astron. Soc.* **467**, 4858–4864.

WALEFFE, F. 1997 On a self-sustaining process in shear flows. *Phys. Fluids* **9**, 883–900.

WILLIS, A. P. & BARENGHI, C. F. 2002 A Taylor-Couette dynamo. *Astron. Astrophys.* **393**, 339–343.

WILLIS, A. P., CVITANOVIC, P. & AVILA, M. 2013 Revealing the state space of turbulent pipe flow by symmetry reduction. *J. Fluid Mech.* **721**, 514–540.

YOUSEF, T. A., HEINEMANN, T., SCHEKOCHIHIN, A. A., KLEEORIN, N., ROGACHEVSKII, I, ISKAKOV, A. B., COWLEY, S. C. & MCWILLIAMS, J. C. 2008*a* Generation of magnetic field by combined action of turbulence and shear. *Phys. Rev. Lett.* **100**, 184501.

YOUSEF, T. A., HEINEMANN, T., RINCON, F., SCHEKOCHIHIN, A. A., KLEEORIN, N., ROGACHEVSKII, I, COWLEY, S. C. & MCWILLIAMS, J. C. 2008*b* Numerical experiments on dynamo action in sheared and rotating turbulence. *Astron. Nachr.* **329** (7), 737–749.

ZEL'DOVICH, Y. B. 1957 The magnetic field in the two-dimensional motion of a conducting turbulent fluid. *Sov. Phys. JETP* **4**, 460–462.

https://doi.org/10.1017/jfm.2019.990 Published online by Cambridge University Press